

AN INVERSE SOURCE PROBLEM OF THE POISSON EQUATION WITH CAUCHY DATA

JI-CHUAN LIU

Communicated by Goong Chen

ABSTRACT. In this article, we study an inverse source problem of the Poisson equation with Cauchy data. We want to find iterative algorithms to detect the hidden source within a body from measurements on the boundary. Our goal is to reconstruct the location, the size and the shape of the hidden source. This problem is ill-posed, regularization techniques should be employed to obtain the regularized solution. Numerical examples show that our proposed algorithms are valid and effective.

1. INTRODUCTION

Inverse source problems are very important for applications in science, engineering and bioengineering which have attracted great attention of many researchers in recent years, refer to [6, 10]. In this paper, we consider the problem of determining a source term of the Poisson equation. The inverse source problem consists of determining the location, the size and the shape of the hidden source from available measured data on the boundary. This inverse source problem is nonlinear and ill-posed in the sense that the solution, even if it exists, does not depend continuously on the measured data. Any small errors in the given data might induce large errors in the solution. Thus regularization techniques should be employed in our proposed algorithms.

Inverse source problems of the Poisson equation have been researched extensively [3, 4, 5, 11, 13, 14, 15, 16, 18, 20]. Bubnov, Erokhin and Isakov [5, 16] presented some theoretical results to reconstruct the unknown source or obstacles from overdetermined boundary measurements of solutions of the Poisson equation. Baratchart et al. [4] solved the inverse problem of locating pointwise or small size conductivity defaults in a plane domain from overdetermined boundary measurements of solutions to the Laplace equation. Hon et al. [15, 20] proposed some effective numerical algorithms to solve inverse source problems of the Poisson equation. Hanke and Rundell [11] used the rational approximation method to solve inverse source problems for determining hidden obstacles. There are some iterative

2010 *Mathematics Subject Classification.* 65N20, 65N21.

Key words and phrases. Inverse source problem; gradient descent method; trust-region-reflective algorithm; Poisson equation; ill-posed problem.

©2017 Texas State University.

Submitted October 26, 2016. Published May 4, 2017.

algorithms for obtaining source parameters from measurement data on the boundary [13, 14, 18, 22, 23]. Hettlich and Rundell [14] applied iterative algorithms to solve an inverse potential problem for reconstruction the shape of an obstacle.

In this paper, we propose two reconstruction algorithms to solve an inverse source problem of the Poisson equation from measurements on the boundary. According to the fundamental solution of Laplace equation, we can obtain the expression of solution for inverse boundary value problem with boundary integral equation. Based on the shape derivative, we apply gradient descent algorithm (GDA) and trust-region-reflective algorithm (TRA) to detect the location, the size and the shape of the hidden source within a body. From numerical experiments, we can see that the proposed iterative algorithms are feasible and stable.

The outline of the paper is as follows. In Section 2, we introduce an inverse source problem of the Poisson equation. We introduce the shape derivative and parameterization of boundary in Section 3. We propose both reconstruction algorithms to detect the hidden source within a body in Section 4. In Section 5, we give some examples to illustrate the efficiency of the proposed reconstruction algorithms.

2. FORMULATION OF AN INVERSE SOURCE PROBLEM

The inverse source problem we consider consists in detecting the location, the size and the shape of the hidden source of the Poisson equation from a single measurement pair of Cauchy data on the boundary. Assume that Ω is a simply connected bounded domain of \mathbb{R}^2 with a smooth boundary $\partial\Omega$, and Ω^* is a subdomain of Ω whose boundary Γ is piecewise differentiable and star-like. We consider the inverse source problem in the following

$$\Delta u = f, \quad \text{in } \Omega, \quad (2.1)$$

$$u = 0, \quad \text{on } \partial\Omega, \quad (2.2)$$

$$\frac{\partial u}{\partial \nu} = g \quad \text{on } \partial\Omega, \quad (2.3)$$

where ν denotes the outward unit normal to $\partial\Omega$. In this paper, we assume the source term $f \in L^2(\Omega)$ is piecewise constant which has compact support and satisfies $\text{supp } f \subset \Omega^*$.

Note that we have assumed homogeneous Dirichlet values and this can be done without loss of generality, refer to [11]. The inverse source problem is that of recovering f given g . According to the Green's function, we can obtain the expression of the solution of problem (2.1) and (2.2) for $f = \chi(\Omega^*)$ as follows

$$u(x, \chi(\Omega^*)) = \int_{\Omega} G(x, y) f(y) dy = \int_{\Omega^*} G(x, y) dy, \quad x \in \Omega, \quad (2.4)$$

where the Green's function $G : \Omega \times \Omega \rightarrow \mathbb{R}$, is

$$G(x, y) = \begin{cases} \frac{1}{2\pi} (\log |x - y| - \log |\frac{x}{|x|} - |x|y|), & y \neq 0, \\ \frac{1}{2\pi} \log |x|, & y = 0, \end{cases}$$

where $x, y \in \Omega$.

The research of uniqueness of the inverse problem (2.1)-(2.3) has attracted a good deal of attention [16, 14, 17]. From [16], we know that the subdomain domain

Ω^* is x_1 -convex. Therefore we have the uniqueness theorem of the inverse source problem (2.1)-(2.3) as follows

Theorem 2.1 ([16]). *Suppose that either (1) Ω_1^* and Ω_2^* are star-shaped with respect to their centers of gravity, or (2) Ω_1^* and Ω_2^* are convex in x_1 . If $u(\cdot, \chi(\Omega_1^*)) = u(\cdot, \chi(\Omega_2^*))$ on $\Omega \setminus \Omega^*$, then $\Omega_1^* = \Omega_2^*$.*

For the inverse problem (2.1)-(2.3), we want to recover a star-shaped domain $\Omega^* = \{x : |x - a| < w((x - a)/|x - a|)\}$ from the modulo of its potential gradient $|\nabla u(\cdot; \chi_{\Omega^*})|$ given on the hypersurface $\Gamma(h) = \{y : |y| = 1, 1 - h < y_1\}$ where h is a number from $(0, 1)$. We may assume that these centers of gravity are the origin, then the star-shaped domain $\Omega_j^* = \{x : |x| < w_j(x/|x|)\} = \{r < w_j(\sigma)\}$. For a number p , $0 < p < 1$, $|w_j|_{2+p}(\Sigma)$ is the usual Hölder norm for a function w on the unit sphere Σ . For estimating a solution Ω of the inverse domain problem, we have the following stability theorem from [16].

Theorem 2.2 ([16, Chap.2]). *Suppose $b < w_j < 1 - b$ on Σ where $0 < b < 1$. There is a constant C depending only on $|w_j|_{2+p}(\Sigma)$, b and h such that if*

$$\|\nabla u(\cdot; \chi_{\Omega_1^*}) - \nabla u(\cdot; \chi_{\Omega_2^*})\|_{L^2(\Gamma(h))} < \varepsilon,$$

then

$$|w_1 - w_2| < C |\ln \varepsilon|^{-1/C} \quad \text{on } \Sigma.$$

Tikhonov first applied this result to show a stability in the inverse problem of potential theory, refer to [25] for details. From the above theorems 2.1 and 2.2, we know that the solution of inverse problem (2.1)-(2.3) is unique and stable.

From (2.4), we can get

$$\frac{\partial u(x, \chi(\Omega^*))}{\partial \nu(x)} = \int_{\Omega} \frac{\partial G(x, y)}{\partial \nu(x)} f(y) dy, \quad x \in \partial \Omega. \quad (2.5)$$

Combined (2.3) with (2.5), we can define an operator $\mathcal{A} : L^2(\Omega) \rightarrow L^2(\partial \Omega)$, satisfying

$$\mathcal{A}f = g, \quad (2.6)$$

where

$$\mathcal{A}f = \int_{\Omega} \frac{\partial G(x, y)}{\partial \nu(x)} f(y) dy, \quad x \in \partial \Omega, \quad (2.7)$$

According to (2.7), we know that \mathcal{A} is a compact linear operator. The problem of solving (2.6) is ill-posed, refer to [26] for detail, that is the solution, if exists, does not depend continuously on the data g . Therefore, it is impossible to solve this inverse source problem using classical numerical methods.

In this article, we want to determine the location, the size and the shape of the hidden source within a body. However, we can obtain the measurements g^δ in the real application, i.e.,

$$\|g^\delta - g\|_{L^2(\partial \Omega)} \leq \delta, \quad (2.8)$$

where $\|\cdot\|_{L^2(\partial \Omega)}$ is the L^2 -norm on the boundary and δ is a noisy level.

Instead of (2.6), one solves the regularized equation

$$(\mathcal{A}\mathcal{A}^* + \lambda)f = \mathcal{A}^*g^\delta. \quad (2.9)$$

The equation (2.9) is the Euler equation for the problem of minimization of the functional

$$\frac{1}{2} \|\mathcal{A}f - g^\delta\|_{L^2(\partial \Omega)}^2 + \frac{\lambda}{2} \|f\|_{L^2(\Omega)}^2, \quad (2.10)$$

which is the famous Tikhonov regularization method [26].

Thus we can obtain the convergence theorem as follows, refer to [16],

Theorem 2.3. *For each $\lambda > 0$ there is a solution f^λ to the minimization (2.10) and any such solution satisfies the estimate*

$$\|f^\lambda - f\|_{L^2(\Omega)} \leq \omega^\lambda(2\|g^\delta - g\|_{L^2(\partial\Omega)} + \sqrt{\lambda})$$

provided \mathcal{A} is one-to-one, where ω^λ is a function such that $\omega^\lambda \rightarrow 0$ when $\lambda \rightarrow 0$.

3. SHAPE DERIVATIVE AND PARAMETERIZATION

3.1. Eulerian derivative of a shape functional. We want to study the geometric change of a bounded domain Ω^* which is thought to be a collection of material particles changing their position in time. The space occupied by them at time will determine a new configuration Ω_σ^* . The change in the geometry of Ω^* will be given by a process which deforms the initial configuration Ω^* . To formalize this mathematically, let domain $\Omega^* \subset \mathbb{R}^2$ be bounded with Lipschitz boundary Γ , and transformations $\Lambda_\sigma : \Omega^* \rightarrow \mathbb{R}^2, \sigma \in [0, \varepsilon]$, i.e.,

$$y^* \in \Omega^* \mapsto y = \Lambda_\sigma(y^*) \equiv y(\sigma, y^*), \quad (3.1)$$

where Λ_σ is bijection and $\Lambda_\sigma \in C^1(\Omega^*)$. Then we can get the transformed geometry as follows

$$\Omega_\sigma^* = \Lambda_\sigma(\Omega^*), \quad (3.2)$$

i.e., Ω_σ^* is the image of Ω^* with respect to Λ_σ .

Definition 3.1. [19] For the point $y(\sigma)$, the Eulerian velocity field $\vec{h}(\sigma, y)$ is as follows

$$\vec{h}(\sigma, y) = \frac{\partial y}{\partial \sigma}(\sigma, \Lambda_\sigma^{-1}(y)). \quad (3.3)$$

From the above definition 3.1, it can be seen that $y(\sigma, y^*)$ satisfies an initial value problem

$$\begin{aligned} \frac{d}{d\sigma} y(\sigma, y^*) &= \vec{h}(\sigma, y(\sigma, y^*)), \\ y(0, y^*) &= y^*, \end{aligned} \quad (3.4)$$

conversely, according to transformations $\Lambda_\sigma(y; \vec{h})$, we can obtain the solution of problem (3.4) for $\vec{h}(\sigma, y)$.

Based on the Eulerian velocity field \vec{h} , we introduce a directional derivative for a shape functional.

Definition 3.2 ([19]). Let J be a functional with $\Omega^* \mapsto J(\Omega^*), \Omega^* \subset \mathbb{R}^2$. Then the Eulerian derivative of the functional J at Ω^* in the direction of a vector field \vec{h} is given by

$$dJ(\Omega^*; \vec{h}) = \frac{d}{d\sigma} J(\Omega_\sigma) \Big|_{\sigma=0} = \lim_{\sigma \rightarrow 0} \frac{1}{\sigma} (J(\Omega_\sigma^*) - J(\Omega^*)), \quad (3.5)$$

where $\Omega_\sigma^* = \Lambda_\sigma(\Omega^*; \vec{h})$.

From definition 3.2, we know that if $dJ(\Omega^*; \vec{h})$ exists for all \vec{h} , then the Eulerian derivative is said to be a shape derivative.

3.2. Shape derivatives of a volume integral. Now we consider the shape derivative of a volume integral. The domain function is given by the volume integral of a function $\varphi \in W_{loc}^{1,1}(\mathbb{R}^2)$

$$J(\Omega_\sigma^*) = \int_{\Omega_\sigma^*} \varphi dy. \tag{3.6}$$

We recall from [24, 1] the following transformation Lemmas.

Lemma 3.3. *Let $\varphi \in W_{loc}^{1,1}(\mathbb{R}^2)$, then $\varphi \circ \Lambda_\sigma \in W_{loc}^{1,1}(\mathbb{R}^2)$ and*

$$J(\Omega_\sigma^*) = \int_{\Omega_\sigma^*} \varphi dy = \int_{\Omega^*} \varphi \circ \Lambda_\sigma J_\sigma dy, \tag{3.7}$$

where $J_\sigma = \det \mathfrak{D}\Lambda_\sigma$ is the volume jacobian.

Lemma 3.4. (1) *For σ small enough, the map $W_{loc}^{1,1}(\mathbb{R}^2) \rightarrow W_{loc}^{1,1}(\mathbb{R}^2); \varphi \mapsto \varphi \circ \Lambda_\sigma$ is locally lipschitz and*

$$\nabla(\varphi \circ \Lambda_\sigma) = (\mathfrak{D}\Lambda_\sigma)^T (\nabla\varphi) \circ \Lambda_\sigma, \tag{3.8}$$

(2) *If Λ_σ is the flow of a vector field $\vec{h} \in C^0([0, \varepsilon), C^1(\mathbb{R}^2, \mathbb{R}^2))$, then the map $[0, \varepsilon) \rightarrow W_{loc}^{1,1}(\mathbb{R}^2); \sigma \mapsto \varphi \circ \Lambda_\sigma$ is well defined and*

$$\frac{d}{d\sigma}(\varphi \circ \Lambda_\sigma) = (\nabla\varphi \cdot \vec{h}(\sigma)) \circ \Lambda_\sigma \in L_{loc}^1(\mathbb{R}^2); \tag{3.9}$$

the map $[0, \varepsilon) \rightarrow C_{loc}^0(\mathbb{R}^2); \sigma \mapsto J_\sigma$ is differentiable with

$$\frac{d}{d\sigma} J_\sigma = (\operatorname{div} \vec{h}(\sigma)) \circ \Lambda_\sigma J_\sigma \in C_{loc}^0(\mathbb{R}^2). \tag{3.10}$$

In terms of definition 3.2 and Lemma 3.3, we can get

$$\begin{aligned} dJ(\Omega^*; \vec{h}) &= \lim_{\sigma \rightarrow 0} \frac{1}{\sigma} \int_{\Omega^*} ((\varphi \circ \Lambda_\sigma) J_\sigma - (\varphi \circ \Lambda_0) J_0) dy \\ &= \int_{\Omega^*} \lim_{\sigma \rightarrow 0} \frac{1}{\sigma} ((\varphi \circ \Lambda_\sigma) J_\sigma - (\varphi \circ \Lambda_0) J_0) dy, \end{aligned} \tag{3.11}$$

where $\Lambda_0(y) = y$ and $J_0(y) = 1$.

From Lemma 3.4, we apply product rule, chain rule and Gauss theorem to have

$$\begin{aligned} dJ(\Omega^*; \vec{h}) &= \int_{\Omega^*} ((\nabla\varphi \cdot \vec{h}(0)) \circ \Lambda_0 J_0 + (\varphi \circ \Lambda_0)(\operatorname{div} \vec{h}(0)) \circ \Lambda_0 J_0) dy \\ &= \int_{\Omega^*} (\nabla(\varphi \circ \Lambda_0) \cdot \vec{h}(0) + (\varphi \circ \Lambda_0)(\operatorname{div} \vec{h}(0) \circ \Lambda_0)) dy \\ &= \int_{\Omega^*} (\nabla\varphi \cdot \vec{h}(0) + \varphi \operatorname{div} \vec{h}(0)) dy \\ &= \int_{\Omega^*} \operatorname{div}(\varphi \vec{h}(0)) dy \\ &= \int_{\Omega^*} \varphi \vec{h}(0) \cdot \nu d\Gamma, \end{aligned} \tag{3.12}$$

where $\vec{h}(0) \cdot \nu$ is the Euclidean inner product in \mathbb{R}^2 , Γ is the boundary of Ω^* , ν is the outward unit normal of the boundary Γ .

Theorem 3.5. Let $\varphi \in W_{\text{loc}}^{1,1}(\mathbb{R}^2)$, Λ_σ be the flow of a vector field \vec{h} in the space $C^0([0, \varepsilon], C^1(\mathbb{R}^2, \mathbb{R}^2))$, the open subset Ω^* has a Lipschitz boundary Γ , ν is the outward unit normal of the boundary Γ , then the shape derivatives of a volume integral is as follows

$$dJ(\Omega^*; \vec{h}) = \int_{\Gamma} \varphi \vec{h}(0) \cdot \nu d\Gamma. \quad (3.13)$$

In terms of Theorem 3.5, we can get the shape derivative of solution for problem (2.1) and (2.2) from (2.4)

$$du(x, \Omega^*; \vec{h}) = \int_{\Gamma} G(x, y) \vec{h}(0, y) \cdot \nu(y) d\Gamma(y), \quad x \in \Omega^*. \quad (3.14)$$

3.3. Parameterization. To compute easily, we should parameterize the boundary Γ of Ω^* . We want to detect the location and the size of the hidden source, and then reconstruct the shape of the source. Thus we employ two methods to parameterize the boundary Γ .

Firstly, we apply the polar coordinates to parameterize the boundary Γ given by

$$\Gamma : O + r(\cos t, \sin t), 0 \leq t \leq 2\pi,$$

for determining the location and the size of the hidden source within a body, where $O = (O_1, O_2)$ is the centroid of the domain Ω^* and r is radius. We take every point y on the boundary Γ of the domain Ω^* . Let

$$y = \begin{pmatrix} O_1 \\ O_2 \end{pmatrix} + r \begin{pmatrix} \cos t \\ \sin t \end{pmatrix}, \quad 0 \leq t \leq 2\pi.$$

We take three transformations $\Lambda_{\sigma_1}, \Lambda_{\sigma_2}, \Lambda_{\sigma_3}$ for O_1, O_2 and r , respectively, then we can get the transformed geometry Ω_σ^* . Three transformations $\Lambda_{\sigma_1}, \Lambda_{\sigma_2}$ and Λ_{σ_3} are given by

$$\Lambda_{\sigma_1}(y) = y + \sigma_1 \begin{pmatrix} 1 \\ 0 \end{pmatrix}, \quad \Lambda_{\sigma_2}(y) = y + \sigma_2 \begin{pmatrix} 0 \\ 1 \end{pmatrix}, \quad \Lambda_{\sigma_3}(y) = y + \sigma_3 \begin{pmatrix} \cos t \\ \sin t \end{pmatrix}.$$

Thus the vector field $\vec{h}(0, y) = (h_1, h_2, h_3)$ is as follows

$$h_1 = \begin{pmatrix} 1 \\ 0 \end{pmatrix}, \quad h_2 = \begin{pmatrix} 0 \\ 1 \end{pmatrix}, \quad h_3 = \begin{pmatrix} \cos t \\ \sin t \end{pmatrix}. \quad (3.15)$$

By using a simple calculation, we obtain

$$\begin{aligned} \frac{d\Lambda_{\sigma_1}(y)}{d\sigma_1} \Big|_{\sigma_1=0} &= \frac{d\Lambda_{\sigma_1}(y)}{dO_1} = h_1, & \frac{d\Lambda_{\sigma_2}(y)}{d\sigma_2} \Big|_{\sigma_2=0} &= \frac{d\Lambda_{\sigma_2}(y)}{dO_2} = h_2, \\ \frac{d\Lambda_{\sigma_3}(y)}{d\sigma_3} \Big|_{\sigma_3=0} &= \frac{d\Lambda_{\sigma_3}(y)}{dr} = h_3. \end{aligned}$$

Let $y = (y_1, y_2)$, we know that

$$y'_1 = \frac{dy_1}{dt} = -r \sin t, \quad y'_2 = \frac{dy_2}{dt} = r \cos t.$$

So the outward unit normal is

$$\nu = \frac{(y'_2, -y'_1)}{\sqrt{(y'_1)^2 + (y'_2)^2}} = (\cos t, \sin t). \quad (3.16)$$

We can use $\beta = (O_1, O_2, r)$ to describe the location and the size of the hidden source within a body.

Secondly, in order to reconstruct the shape of the hidden source, we parameterize the boundary Γ of Ω^* as

$$\Gamma : O + r(t)(\cos t, \sin t), 0 \leq t \leq 2\pi,$$

where O is the centroid of the domain Ω^* which is fixed, and $r(t)$ is a real-valued function of $0 \leq t \leq 2\pi$ which is given by

$$r(t) = c_0 + \sum_{j=1}^l (c_j \cos(jt) + c_{j+l} \sin(jt)), \quad (3.17)$$

where $0 \leq t \leq 2\pi$, $c_j \in \mathbb{R}$, $l \in \mathbb{N}$.

We take every point y on the boundary Γ of the domain Ω^* . Let

$$y = O + r(t) \begin{pmatrix} \cos t \\ \sin t \end{pmatrix},$$

We take transformations $\Lambda_{\sigma_0}, \dots, \Lambda_{\sigma_{2l}}$ for c_0, \dots, c_{2l} , respectively, then we can get the transformed geometry $\Omega_{\sigma_j}^*$. Transformations $\Lambda_{\sigma_0}, \dots, \Lambda_{\sigma_{2l}}$ are given by

$$\Lambda_{\sigma_j}(y) = y + r_{\sigma_j}(t) \begin{pmatrix} \cos t \\ \sin t \end{pmatrix}, \quad j = 0, 1, \dots, 2l,$$

where

$$r_{\sigma_j}(t) = (c_0, \dots, c_j + \sigma_j, \dots, c_{2l})(1, \dots, \cos(lt), \sin(lt), \dots, \sin(lt))^T,$$

$0 \leq t \leq 2\pi$. The vector field $\vec{h} = (h_0, h_1, \dots, h_{2l})$ is given by

$$\begin{aligned} h_j &= \cos(jt) \begin{pmatrix} \cos t \\ \sin t \end{pmatrix}, \quad j = 0, \dots, l, \\ h_j &= \sin((j-l)t) \begin{pmatrix} \cos t \\ \sin t \end{pmatrix}, \quad j = l+1, \dots, 2l, \end{aligned} \quad (3.18)$$

and we have

$$\left. \frac{d\Lambda_{\sigma_j}(y)}{d\sigma_j} \right|_{t=0} = \frac{d\Lambda_{\sigma_j}(y)}{dc_j} = h_j, \quad j = 0, \dots, 2l.$$

Let $y = (y_1, y_2) = O + r(t)(\cos t, \sin t)$, we obtain

$$\begin{aligned} y'_1 &= \frac{dy_1}{dt} = r'(t) \cos t - r(t) \sin t, \\ y'_2 &= \frac{dy_2}{dt} = r'(t) \sin t + r(t) \cos t. \end{aligned}$$

Thus the outward unit normal vector is given by

$$\nu = \frac{(y'_2, -y'_1)}{\sqrt{(y'_1)^2 + (y'_2)^2}}. \quad (3.19)$$

We can use $\beta = (c_0, c_1, \dots, c_{2l})$ to describe the shape of the hidden source within a body.

According to parameters β and the vector field \vec{h} , Equation (3.14) can be changed as

$$\begin{aligned} \nabla_{\beta} u(x, \beta; \vec{h}) &= \int_0^{2\pi} G(x, O_1 + r \cos t, O_2 + r \sin t) \vec{h}(0, O_1 + r \cos t, O_2 + r \sin t) \\ &\quad \times \nu(O_1 + r \cos t, O_2 + r \sin t) \sqrt{(y'_1)^2 + (y'_2)^2} dt, \quad x \in \Omega \end{aligned} \quad (3.20)$$

where $\vec{h} = (h_1, h_2, h_3)^T$ or $\vec{h} = (h_0, \dots, h_{2l})^T$.

Denote $u(x, \chi(\Omega^*))$ and $\nabla_\beta u(x, \beta; \vec{h})$ as $u(x, \beta)$ and $\nabla_\beta u(x, \beta)$, respectively. Using polar coordinate to (2.4), we have

$$u(x, \beta) = \int_0^{2\pi} dt \int_0^{r(t)} \partial G(x, y(O_1 + r \cos t, O_2 + r \sin t)) r dr, \quad x \in \Omega, \quad (3.21)$$

and

$$\begin{aligned} & \nabla_\beta u(x, \beta) \\ &= \int_0^{2\pi} G(x, O_1 + r(t) \cos t, O_2 + r(t) \sin t) \vec{h}(0, O_1 + r(t) \cos t, O_2 \\ & \quad r(t) \sin t) \cdot \nu(O_1 + r(t) \cos t, O_2 + r(t) \sin t) \sqrt{(y'_1)^2 + (y'_2)^2} dt, \quad x \in \Omega, \end{aligned} \quad (3.22)$$

then we can get

$$\begin{aligned} & \frac{\partial u(x, \beta)}{\partial \nu(x)} \\ &= \int_0^{2\pi} dt \int_0^{r(t)} \frac{\partial G(x, y(O_1 + r \cos t, O_2 + r \sin t))}{\partial \nu(x)} r dr \\ &= \int_0^{2\pi} dt \int_0^1 \frac{\partial G(x, y(O_1 + vr(t) \cos t, O_2 + vr(t) \sin t))}{\partial \nu(x)} vr^2(t) dv, \quad x \in \Omega, \end{aligned} \quad (3.23)$$

$$\begin{aligned} & \frac{\partial \nabla_\beta u(x, \beta)}{\partial \nu(x)} \\ &= \int_0^{2\pi} \frac{\partial G(x, O_1 + r(t) \cos t, O_2 + r(t) \sin t)}{\partial \nu(x)} \vec{h}(0, O_1 + r(t) \cos t, O_2 \\ & \quad + r(t) \sin t) \cdot \nu(O_1 + r(t) \cos t, O_2 + r(t) \sin t) \sqrt{(y'_1)^2 + (y'_2)^2} dt, \quad x \in \Omega. \end{aligned} \quad (3.24)$$

4. RECONSTRUCTION ALGORITHMS FOR A HIDDEN SOURCE

In this section, we want to seek reconstruction algorithms to determine the location, the size and the shape of hidden source. In practical applications, we can only get measured data with errors on the boundary. The inverse source problem is nonlinear and ill-posed. Therefore, we should employ the regularization technique to solve this inverse source problem.

We consider the objective function as follows

$$F(\beta) = \frac{1}{2} \left\| g^\delta - \frac{\partial u(\cdot, \beta)}{\partial \nu} \right\|_{L^2(\partial\Omega)}^2, \quad (4.1)$$

where $\|\cdot\|_{L^2(\partial\Omega)}$ denotes the L^2 -norm, g^δ are the measured data on the boundary of the domain Ω and

$$\beta = (O_1, O_2, r) \in \mathbb{R}^3, \quad \text{or} \quad \beta = (c_0, \dots, c_{2l}) \in \mathbb{R}^{(2l+1)}.$$

This problem is a nonlinear least squares optimization problem, we propose reconstruction algorithms to find the minimum of the objective function in (4.1) by update β . Starting with an initial guess β^0 , these algorithms proceed by the iterations

$$\beta^{k+1} = \beta^k + \Delta, \quad k = 0, 1, 2, \dots, \quad (4.2)$$

where Δ is the increment vector.

From (4.1), we can obtain the gradient of the objective function

$$F'(\beta) = -\left\langle g^\delta - \frac{\partial u(\cdot, \beta)}{\partial \nu}, \frac{\partial \nabla_\beta u(\cdot, \beta)}{\partial \nu} \right\rangle, \quad (4.3)$$

where $\langle \cdot, \cdot \rangle$ denotes the $L^2(\partial D)$ inner product.

We know that the measured data g^δ are discrete data at discrete points $\{x_s\}$ on the boundary of the domain Ω . In order to compute numerically inner product (4.3), we apply the collocation method to compute $\frac{\partial u(x, \beta)}{\partial \nu(x)}$ and $\frac{\partial \nabla_\beta u(x, \beta)}{\partial \nu(x)}$ on the collocation points $\{x_s\}$ of the boundary $\partial\Omega$. For each collocation point x_s , we should estimate the integral equations (3.23) and (3.24). We note that the kernels are smooth in (3.23) and (3.24) so that the well-estimated quadrature rules can be employed for numerical approximation.

The interval $[0, 2\pi]$ is partitioned as $0 = t_0 < t_1 < \dots < t_{n_1} < 2\pi$, where $\theta_i = (i-1)h_t$ ($i = 1, \dots, n_1$) and $h_t = \frac{2\pi}{n_1}$. The interval $[0, 1]$ is partitioned as $0 = v_0 < v_1 < \dots < v_{n_2} < 1$, where $v_j = (j-1)h_v$ ($j = 1, \dots, n_2$) and $h_v = \frac{1}{n_2}$. In terms of integral equations (3.23) and (3.24), we can obtain the approximate value of collocation point x_s as follows

$$\begin{aligned} & \frac{\partial u(x_s, \beta)}{\partial \nu(x_s)} \\ &= \sum_{j=1}^{n_2} \left(\sum_{i=1}^{n_1} \frac{\partial G(x_s, y(O_1 + v_j r(t_i) \cos t_i, O_2 + v_j r(t_i) \sin t_i))}{\partial \nu(x_s)} v_j r^2(t_i) h_v \right) h_t, \end{aligned} \quad (4.4)$$

$$\begin{aligned} \frac{\partial \nabla_\beta u(x_s, \beta)}{\partial \nu(x_s)} &= \sum_{i=1}^{n_1} \frac{\partial G(x_s, O_1 + r(t_i) \cos t_i, O_2 + r(t_i) \sin t_i)}{\partial \nu(x_s)} \vec{h}(0, O_1 \\ &+ r(t_i) \cos t_i, O_2 + r(t_i) \sin t_i) \cdot \nu(O_1 + r(t_i) \cos t_i, O_2 \\ &+ r(t_i) \sin t_i) \sqrt{(y'_1)_i^2 + (y'_2)_i^2} h_t. \end{aligned} \quad (4.5)$$

According to the numerical approximation (4.4) and (4.5), we can compute $\frac{\partial u(x, \beta)}{\partial \nu(x)}$ and $\frac{\partial \nabla_\beta u(x, \beta)}{\partial \nu(x)}$ at the collocation points $\{x_s\}$ on the boundary $\partial\Omega$. Then, the inner product (4.3) can be computed well along with measurement data g^δ .

4.1. Gradient descent algorithm (GDA). GDA is a way to find a local minimum of an objective function. The way it works is we start with an initial guess of the solution and we take the gradient of the function at that point. We step the solution in the negative direction of the gradient and we repeat the process. GDA will eventually converge where the gradient is zero. GDA is a first-order optimization algorithm which is recognized as a highly convergent algorithm for finding the minimum of the objective function. We know that this inverse source problem is ill-posed, we employ the regularization technique for GDA because of the measurement data $g^\delta(x)$. The modified objective function is as follows

$$\tilde{\mathcal{F}}(\beta) = F(\beta) + \frac{\lambda}{2} |\beta|^2, \quad (4.6)$$

where λ is the regularization parameter. According to Theorem 2.3, we can obtain the convergence theorem for parameters β by minimizing objective function $\tilde{\mathcal{F}}(\beta)$.

For GDA, a key issue is to choose the regularization parameter λ . A wise choice of regularization parameter is obviously crucial to obtaining useful approximate

solutions to ill-posed problems, there are well-studied techniques for computing a good regularization parameter, such as the discrepancy principle [21], the generalized cross-validation (GCV) [9], the L-curve [12] and so on. In this paper, we are interested in a-posteriori rules λ for choosing the regularization parameter when minimizing $\tilde{F}(\beta)$. Based on discrepancy principle, we apply sequential discrepancy principle [2] to choose the regularization parameter. For prescribed $0 < q < 1$ and $\lambda_0 > 0$, let

$$\Lambda_q := \{\lambda_j | \lambda_j = q^j \lambda_0, j \in \mathbb{Z}\}. \quad (4.7)$$

Given any $\delta > 0$, measured data g^δ and $\tau > 1$, we say that an element $\lambda \in \Lambda_q$ is chosen according to the sequential discrepancy principle, if

$$F(\beta_\lambda^\delta) < \tau\delta < F(\beta_{\lambda/q}^\delta) \quad (4.8)$$

The gradient of $\tilde{\mathcal{F}}(\beta)$ is

$$\tilde{\mathcal{F}}'(\beta) = F'(\beta) + \lambda\beta. \quad (4.9)$$

The increment vector Δ of (4.1) is given by

$$\Delta = -\alpha\tilde{\mathcal{F}}'(\beta), \quad (4.10)$$

where α is the step size of iteration.

The final iteration relationship is as follows

$$\beta^{k+1} = \beta^k - \alpha\tilde{\mathcal{F}}'(\beta^k), k = 0, 1, 2, \dots \quad (4.11)$$

4.2. Trust-region-reflective optimization algorithm (TRA). TRA is a subspace trust-region method and is based on the interior-reflective Newton method described in [7, 8] for the detail. Each iteration involves the approximate solution of a large linear system using method of preconditioned conjugate gradient. TRA is used to minimize a nonlinear function subject to simple bound. TRA exhibits strong convergence properties and global and second-order convergence.

According to the objective function $F(\beta)$, the shape derivative to β is as follows

$$\tilde{\mathcal{F}}'(\beta) = \frac{\partial \nabla_{\beta} u(\cdot, \beta)}{\partial \nu}. \quad (4.12)$$

Assume the increment Δ_* is a solution of a subproblem as follows

$$\min_{\Delta_* \in \mathbb{R}^n} \{\psi(\Delta_*) = \tilde{\mathcal{F}}'(\beta)^T \Delta_* + \frac{1}{2} \Delta_*^T M \Delta_* : |B \Delta_*| \leq w\}, \quad (4.13)$$

where B is a positive diagonal scaling matrix refer to [7, 8], and $w > 0$ is the trust region size, and

$$M(\beta) = \tilde{\mathcal{F}}'(\beta)^T \tilde{\mathcal{F}}'(\beta) + B \text{diag}(\tilde{\mathcal{F}}'(\beta)) \text{diag}(\text{sign}(\tilde{\mathcal{F}}'(\beta))) B.$$

We take the initial descent direction Δ_* as a new starting guess, and then determine the piecewise linear reflective path $p(\alpha)$. Moreover, we obtain an acceptable stepsize α by an approximate piecewise line minimization $F(\beta^k + p(\alpha_k))$, refer to [7] for details.

The final iteration relationship is as follows

$$\beta^{k+1} = \beta^k + p(\alpha_k), k = 0, 1, 2, \dots \quad (4.14)$$

5. NUMERICAL EXPERIMENTS

In this section, we show that the results of some numerical experiments that illustrate the reconstruction algorithms of the previous section. The measured data are given by

$$g^\delta = g(1 + \delta \cdot \text{rand}(\text{size}(g))),$$

where g is the exact data, $\text{rand}(\text{size}(g))$ is a random number uniformly distributed in $[-1, 1]$ and δ is a relative noise level. In order to calculate conveniently, we take a unit circle as the boundary $\partial\Omega$ of the solution domain Ω .

5.1. Sensitivity analysis on the chosen parameter. As we know, the parameter has an important role in our numerical computation. To analyze the sensitivity of the chosen parameter, we suppose the source is circle, the center is located in origin and the radius is 0.3. We parameterize the boundary Γ of Ω as $\Gamma : O+r(\cos t, \sin t), 0 \leq t \leq 2\pi$, along with $\beta = (O_1, O_2, r)$, choose $(0.71, 0.23, 0.02)$ as a test for starting guess and the error is given by $\text{error} = \sqrt{O_1^2 + O_2^2 + (r - 0.3)^2}$.

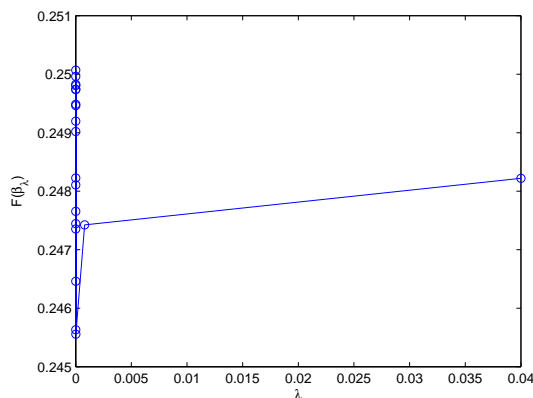


FIGURE 1. Sensitivity of the regularization parameter λ for GDA

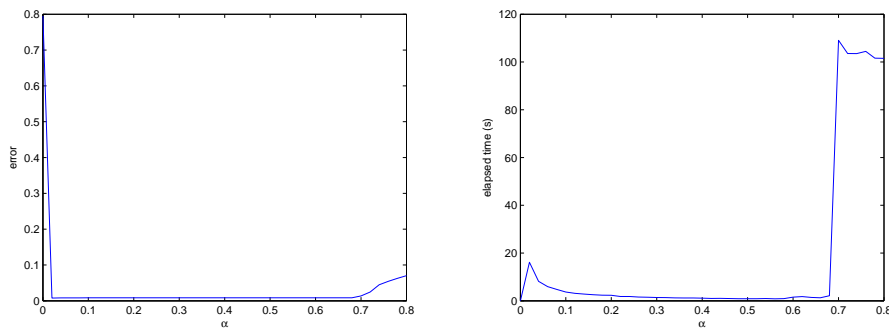


FIGURE 2. Sensitivity of the step size parameter α for GDA

According to the parameter of GDA, the regularization parameter and the step size should be analyzed, the results are shown in Figures 1 and 2. Figure 1 is the sensitivity of the regularization parameter. In this case, we choose $\alpha = 0.25$, $\lambda_0 = 2$, $q = 0.02$, $\tau = 2.46$ and take $|\tilde{\mathcal{F}}(\beta^{k+1}) - \tilde{\mathcal{F}}(\beta^k)| < 10^{-6}$ as a stopping criterion. we apply the sequential discrepancy principle [2] to obtain the regularization parameter $\lambda = 1.6e - 5$ as in Figure 1 shown.

Figure 2 is the sensitivity of the step size. The step size has a consistent increase or decrease effect on the error and the elapsed time of CPU in general. That means, as the error decrease, the elapsed time decrease, at the same time, as the error increase, the elapsed time increase along with the step size increase. In our computation, we want to find the balance between the error and the elapsed time. That means, for fixed the step size α , the error is smaller and the elapsed time of CPU is fewer. Therefore, we choose the step size in the stability interval $[0.2, 0.6]$ from Figures 2(a) and 2(b).

5.2. Numerical stability and convergence of the proposed algorithms. To show the numerical stability and convergence of GDA, we suppose the hidden source is a circle which is located in origin $O(0, 0)$ and the radius is 0.3. We parameterize the boundary Γ of Ω as $\Gamma : O + r(\cos t, \sin t), 0 \leq t \leq 2\pi$, along with $\beta = (O_1, O_2, r)$, choose $(0.71, 0.23, 0.02)$ as a test for starting guess and the error is given by

$$\text{error} = \sqrt{O_1^2 + O_2^2 + (r - 0.3)^2}.$$

In this case, we choose $\alpha = 0.25$, $\lambda_0 = 2$, $q = 0.02$, $\tau = 2.46$ and take $|\tilde{\mathcal{F}}(\beta^{k+1}) - \tilde{\mathcal{F}}(\beta^k)| < 10^{-6}$ as a stopping criterion.

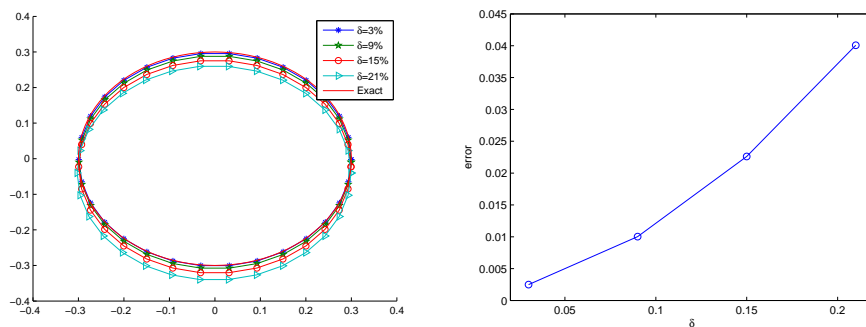


FIGURE 3. The numerical stability of GDA for different noise levels

In Figures 3 and 4, we use GDA to reconstruct the approximation location and the size of hidden source within a body. In Figure 3(a), we investigate the numerical stability of GDA with a fixed number of collocation points and four different levels of noise added to the data, e.g. 3%, 9%, 15% and 21%. Figure 3(b) shows the error of the location and the size between the exact source and the reconstructed source for different noise levels δ . In Figure 4(a), we investigate the numerical convergence of GDA with a fixed level of noise added to the data and four different values of the number of collocation points, e.g. 20, 25, 30, 35, 40. Figure 4(b) shows the error of the location and the size between the exact source and the reconstructed source

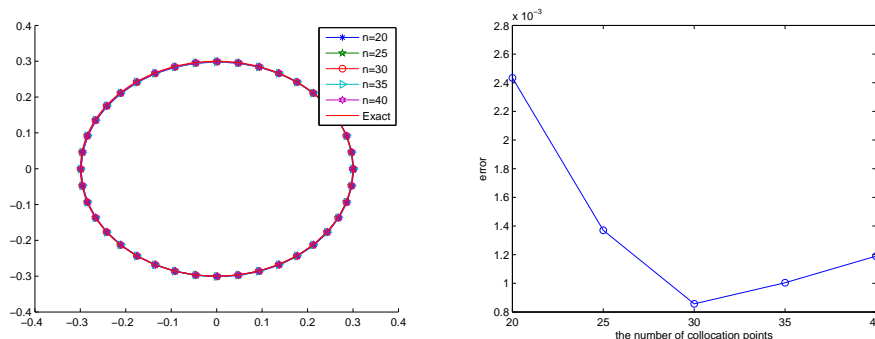


FIGURE 4. The numerical convergence of GDA for different values of the number of collocation points

for the different number of collocation points. From Figures 3 and 4, we can see that our proposed method is stable and effective to detect the hidden source.

5.3. Estimation of the location and the size of the hidden source. To estimate the location and the size of the hidden source within a body, we parameterize the boundary Γ of Ω as $O + \rho(\cos t, \sin t)$, $0 \leq t \leq 2\pi$, along with $\beta = (O_1, O_2, r)$, that is, we use the circle to approximate the source for every iteration.

For simplification, we assume the source is located in origin $(0, 0)$.

Algorithm 1 for GDA Estimate the location and the size of the hidden source.

Let ε , δ , τ , q , λ_0 , α and g^δ be given.

- (1) Input $\beta^0 = (O_1, O_2, r)$: the location and the size of starting guess
- (2) Compute the values of collocation points $\frac{\partial u(\cdot, \beta^k)}{\partial \nu}$ and $\frac{\partial \nabla_{\beta^k} u(\cdot, \beta^k)}{\partial \nu}$ from (4.4) and (4.5)
- (3) Choose λ by the sequential discrepancy principle from (4.8)
- (4) Compute $F'(\beta^k)$ and $\tilde{\mathcal{F}}'(\beta^k)$ from (4.3) and (4.9)
- (5) Update β^{k+1} from (4.11)
- (6) If $\|\tilde{\mathcal{F}}(\beta^{k+1}) - \tilde{\mathcal{F}}(\beta^k)\| \leq \varepsilon$, stop, $\beta = \beta^{k+1}$; otherwise, set $\beta^k = \beta^{k+1}$, return to (4)

Algorithm 2 for TRA Estimate the location and the size of the hidden source.

Let g^δ be given.

- (1) Input $\beta^0 = (O_1, O_2, r)$: the location and the size of starting guess
- (2) Compute the values of collocation points $\frac{\partial u(\cdot, \beta^k)}{\partial \nu}$ and $\frac{\partial \nabla_{\beta^k} u(\cdot, \beta^k)}{\partial \nu}$ from (4.4) and (4.5)
- (3) Compute $R = \|g^\delta - \frac{\partial u(\cdot, \beta^k)}{\partial \nu}\|$ and $J = \tilde{\mathcal{F}}'(\beta^k)$ from (4.12)
- (4) In terms of R and J , call Matlab programs 'lsqnonlin' to update β^{k+1}
- (5) From the updated β^{k+1} , obtain the approximation location (O_1^{k+1}, O_2^{k+1}) and the size r^{k+1} of the hidden source

Example 5.1. In this case, we suppose the source is a peanut or a peach or a pear or a "L" type. Polar radius of the peanut is given by

$$r_{pt} = 0.4\sqrt{(\cos t)^2 + 0.25(\sin t)^2}, \quad 0 \leq t \leq 2\pi,$$

polar radius of the peach is given by

$$r_{ph} = 3/10 - 1/12 \sin t - 1/28 \sin(3t), \quad 0 \leq t \leq 2\pi,$$

polar radius of the pear is given by

$$r_{pr} = 3/10 + 1/16 \cos(3t), \quad 0 \leq t \leq 2\pi,$$

and the longest length of the "L" type is 0.25.

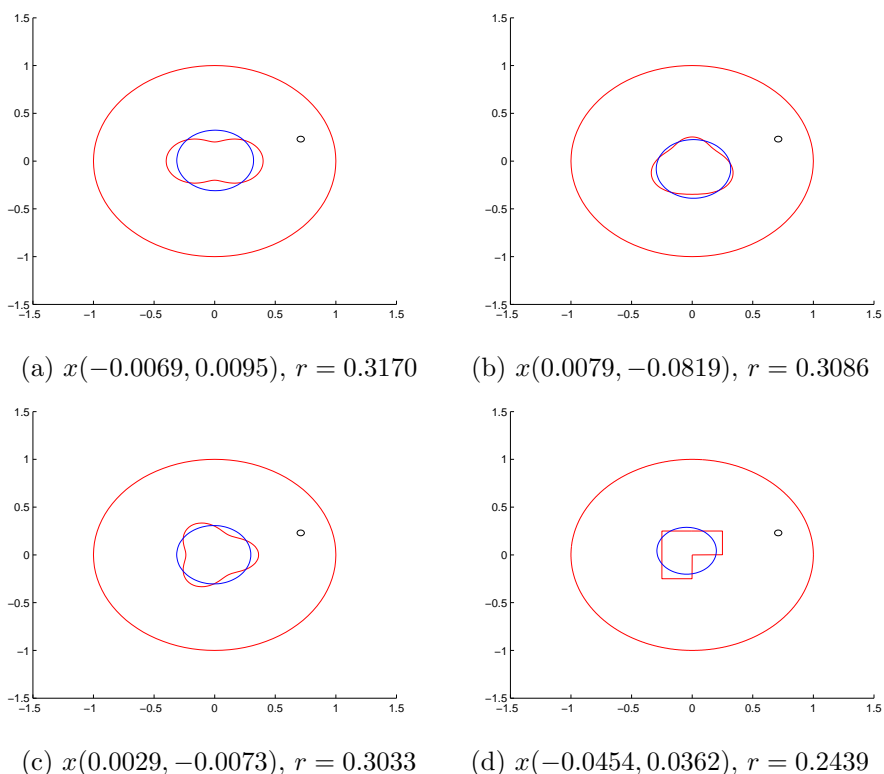


FIGURE 5. (a) Peanut; (b) peach; (c) pear; (d) "L" shape. Estimate the location and the size of the source with 10% noise data along with exact solution (red), initial guess (black) and recovered solution (blue), respectively for Example 5.1.

In Figure 5, we can get the approximate centroid location and the size of the source using GDA along with 30 measured data. We choose $\varepsilon = 10^{-7}$, $\delta = 0.1$, $\alpha = 0.25$, $\lambda_0 = 1.5$, $q = 0.02$ and $\tau = 2.71$. In fact, we can use any point and any radius as a starting guess in the domain of the solution for these four cases. In Figure 5, we choose $(0.71, 0.23, 0.02)$ as a test for starting guess. From Figure 5 and Table 1, it can be seen that we obtain the more accurate approximation of the location and the size for four different cases by GDA. We can get the same result with TRA.

TABLE 1. The approximate location and the size of the hidden source for four different cases using GDA along with 10% noise data for Example 5.1

	Location	Size
Exact	(0,0)	r
Guess	(0.71,0.23)	0.02
peanut	(-0.0069,0.0095)	0.3170
peach	(0.0079,-0.0819)	0.3086
pear	(0.0029,-0.0073)	0.3033
“L” shape	(-0.0454,0.0362)	0.2439

5.4. Estimation of the shape of the hidden source. From the previous subsection, we know that the location and the size of the hidden source can be determined. In this sub-section, we try to reconstruct the shape of the hidden source along with the location and the size of the source given a prior. Therefore, we can parameterize the boundary Γ of Ω as $O + r(t)(\cos t, \sin t)$ with $r(t)$ a real-valued function of $0 \leq t \leq 2\pi$, and O is fixed which is the center of the sub-domain Ω . We apply GDA and TRA to reconstruct the shape of the source.

Algorithm 3 for GDA Reconstruct the shape of the hidden source. Let ε , δ , τ , q , λ_0 , α , O , c_0^0 and g^δ be given.

- (1) Input $\beta^0 = (c_0^0, 0, \dots, 0)$: the shape of starting guess
- (2) Compute the values of collocation points $\frac{\partial u(\cdot, \beta^k)}{\partial \nu}$ and $\frac{\partial \nabla_{\beta^k} u(\cdot, \beta^k)}{\partial \nu}$ from (4.4) and (4.5)
- (3) Choose λ by the sequential discrepancy principle from (4.8)
- (4) Compute $F'(\beta^k)$ and $\tilde{\mathcal{F}}'(\beta^k)$ from (4.3) and (4.9)
- (5) Update β^{k+1} from (4.11)
- (6) If $\|\tilde{\mathcal{F}}(\beta^{k+1}) - \tilde{\mathcal{F}}(\beta^k)\| \leq \varepsilon$, stop, $\beta = \beta^{k+1}$; otherwise, set $\beta^k = \beta^{k+1}$, return to (4)

Algorithm 4 for TRA Reconstruct the shape of the hidden source. Let O , ρ and g^δ be given.

- (1) Input $\beta^0 = (c_0^0, 0, \dots, 0)$: the shape of starting guess
- (2) Compute the values of collocation points $\frac{\partial u(\cdot, \beta^k)}{\partial \nu}$ and $\frac{\partial \nabla_{\beta^k} u(\cdot, \beta^k)}{\partial \nu}$ from (4.4) and (4.5)
- (3) Compute $R = \|g^\delta - \frac{\partial u(\cdot, \beta^k)}{\partial \nu}\|$ and $J = \tilde{\mathcal{F}}'(\beta^k)$ from (4.12)
- (4) In terms of R and J , call Matlab programs 'lsqnonlin' to update β^{k+1}
- (5) From (3.17), obtain the shape of the hidden source base on the update β^{k+1}

Example 5.2. In this case, we also assume the hidden source is a peanut or a peach or a pear or a “L” type with the approximate location and the size given by Table 1 in Example 5.1.

In Figures 6 and 7, we apply two iterative algorithms to recover the shape of the hidden source for four different cases within a body. We choose $\varepsilon = 10^{-7}$, $\delta = 0.1$, $\tau = 2.71$, $q = 0.02$, $\lambda_0 = 1.5$, $\alpha = 0.25$ and $c_0^0 = \rho$ for GDA. We take a circle as a

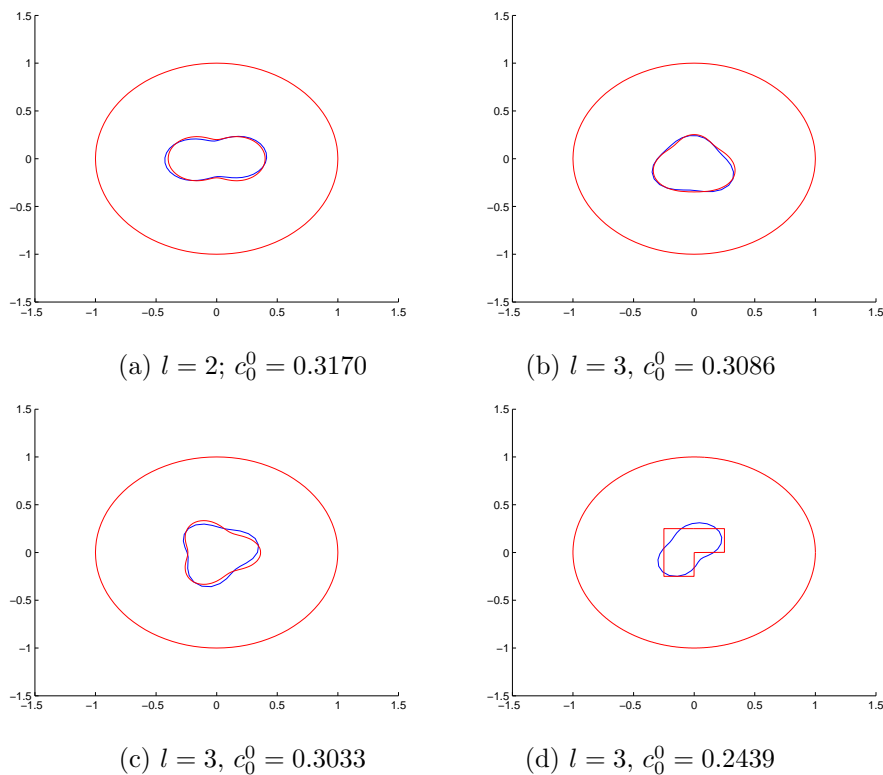


FIGURE 6. (a) Peanut; (b) peach; (c) pear; (d) “L” shape. Reconstructed the shape of the hidden source with 10% noise data using GDA along with exact shape (red) and recovered shape (blue), respectively for Example 5.2.

starting guess for the source, thus we can use the size of the source as the radius of a circle from Table 1, or reset it.

In this example, we use the approximate location given by Table 1 in Example 5.1 as the fix center of the sub-domain Ω and reset the initial value $\beta^0 = (c_0^0, 0, \dots, 0)$ as a starting guess. Compared with these two algorithms, the convergence speed of TRA is much faster than GDA. The run time of CPU for TRA (about 0.5sec) is far less than GDA (about 100sec). From Figures 6 and 7, we can see that these two algorithms work well with noisy data to reconstruct the shape of the source within a body.

Example 5.3. In this case, we consider the hidden source is a kite or a hypocycloid. Polar radius of the kite is given by

$$r_{kt} = 0.3(1 + 0.9 \cos t + 0.15 \sin(2t))/(1 + 0.7 \cos t), 0 \leq t \leq 2\pi, \quad (5.1)$$

and polar radius of the hypocycloid is given by

$$r_{hy} = 0.3\sqrt{10/9 + 2/3 \cos(4t)}, 0 \leq t \leq 2\pi. \quad (5.2)$$

In Figure 8, we apply GDA and TRA to recover the shape of the hidden source along with 10% noise. The centroid of the source is origin. We choose $\varepsilon = 10^{-7}$,

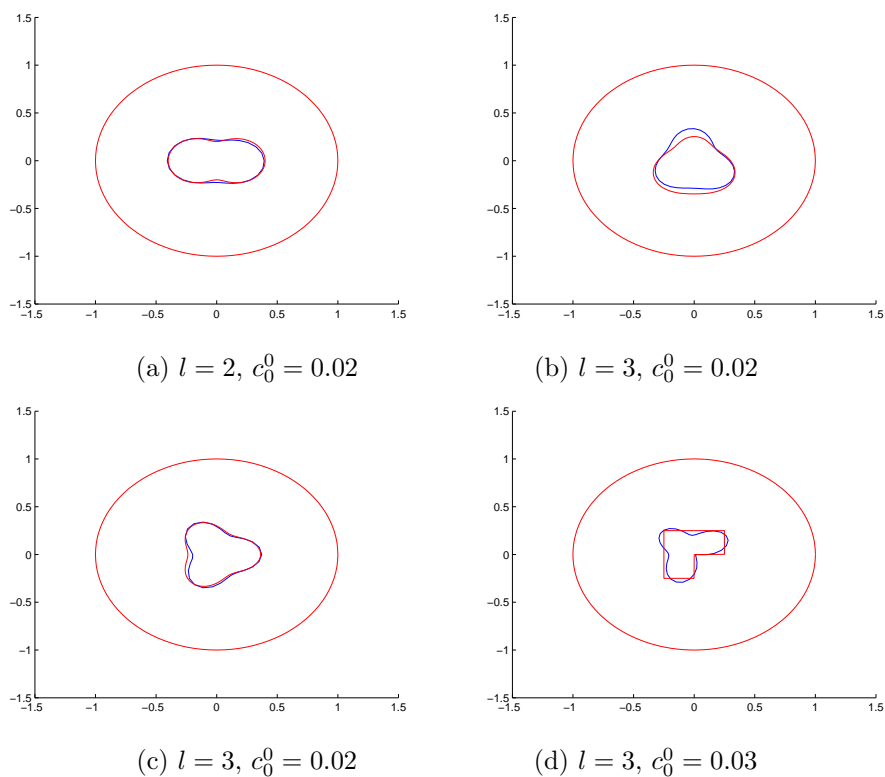


FIGURE 7. (a) Peanut; (b) peach; (c) pear; (d) “L” shape. Reconstructed the shape of the hidden source with 10% noise data using TRA along with exact shape (red) and recovered shape (blue), respectively for Example 5.2.

$\delta = 0.1$, $\tau = 2.12$, $q = 0.02$, $\lambda_0 = 1.2$ and $\alpha = 0.25$ for GDA. GDA is employed to recover the shape of the source in Figures 8(a) and 8(c). The shape of the source in Figures 8(b) and 8(d) is reconstructed by TRA. From Figure 8 we know that TRA is much less sensitive to the noise level, it works with much less prior information. However, the shape of the recovered hidden source agrees well with that of the true one for both iterative algorithms.

Conclusions. In this paper, we consider the inverse source problem within a body from the measured data. We want to detect the salient features of the hidden source, such as the location, the size and the shape. We transform this problem into an optimization problem for finding a minimum of an objective function. This inverse source problem is nonlinear and ill-posed, thus regularization technique of our proposed algorithms should be considered. We apply GDA and TRA to solve this inverse source problem. Our proposed algorithms are robust in the presence of noise, and less sensitive to the noise level and an initial guess. Another nice feature of TRA is that it is self-adaptive, that is, at each iteration it can remedy the possible errors from the previous iterations. Numerical results show that our proposed algorithms are feasible and stable.

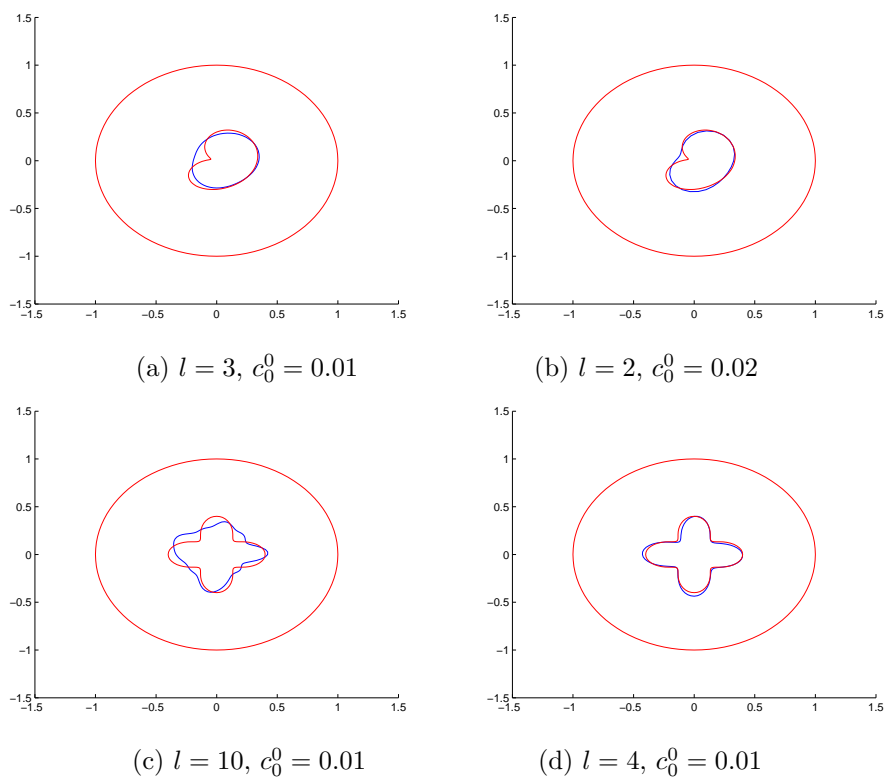


FIGURE 8. Reconstructed the shape of the hidden source with 10% noise data using GDA and TRA along with exact shape (red) and recovered shape (blue), respectively for Example 5.3.

Acknowledgments. The research of Ji-Chuan Liu was supported by the Fundamental Research Funds for the Central Universities (2014QNA57) and the NSF of China (11601512).

REFERENCES

- [1] G. Allaire; *Shape optimization by the homogenization method*, vol. 146, Springer, 2002.
- [2] S. W. Anzengruber, B. Hofmann, P. Mathé; *Regularization properties of the discrepancy principle for tikhonov regularization in banach spaces*, Techn. Univ., Fak. Mathematik, 2012.
- [3] A. E. Badia, T. Ha-Duong; *An inverse source problem in potential analysis*, Inverse Problems **16** (2000), 651.
- [4] L. Baratchart, A. B. Abda, F. B. Hassen, J. Leblond; *Recovery of pointwise sources or small inclusions in 2D domains and rational approximation*, Inverse problems **21** (2005), no. 1, 51.
- [5] B. A. Bubnov, G. N. Erokhin; *Inverse and ill-posed sources problems*, vol. 9, Vsp, 1997.
- [6] M. Cheney, D. Isaacson, J. C. Newell; *Electrical impedance tomography*, SIAM review (1999), 85–101.
- [7] T. F. Coleman, Y. Li; *On the convergence of interior-reflective newton methods for nonlinear minimization subject to bounds*, Mathematical programming **67** (1994), no. 1, 189–224.
- [8] T. F. Coleman, Y. Li; *An interior, trust region approach for nonlinear minimization subject to bounds*, SIAM Journal on Optimization, **6** (1996), 418–445.
- [9] H. G. Gene, M. T. Heath, G. Wahba; *Generalized Cross-Validation as a Method for Choosing a Good Ridge Parameter*, Technometrics **21** (1979), 215–223.

- [10] M. Hämäläinen, R. Hari, R. J. Ilmoniemi, J. Knuutila, O. V. Lounasmaa; *Magnetoencephalography theory, instrumentation, and applications to noninvasive studies of the working human brain*, Reviews of Modern Physics **65** (1993), 413–497.
- [11] M. Hanke, W. Rundell; *On rational approximation methods for inverse source problems*, Inverse Problems and Imaging **5** (2011), no. 1, 185–202.
- [12] P. C. Hansen; *Rank-deficient and discrete ill-posed problems: Numerical aspects of linear inversion*, Society for Industrial and Applied Mathematics, Philadelphia, PA, USA, 1998.
- [13] B. He, T. Musha, Y. Okamoto, S. Homma, Y. Nakajima, T. Sato; *Electric dipole tracing in the brain by means of the boundary element method and its accuracy*, Biomedical Engineering, IEEE Transactions on **BME-34** (1987), no. 6, 406–414.
- [14] F. Hettlich, W. Rundell; *Iterative methods for the reconstruction of an inverse potential problem*, Inverse problems **12** (1999), no. 3, 251.
- [15] Y. C. Hon, M. Li, Y.A. Melnikov; *Inverse source identification by Green's function*, Engineering Analysis with Boundary Elements **34** (2010), no. 4, 352–358.
- [16] V. Isakov; *Inverse source problems*, no. 34, American Mathematical Soc., 1990.
- [17] V. Isakov; *Inverse problems for partial differential equations*, Applied Mathematical Sciences, vol. 127, Springer-Verlag, New York, second edition, 2006.
- [18] R. N. Kavanagh, T. M. Darcey, D. Lehmann, D. H. Fender; *Evaluation of methods for three-dimensional localization of electrical sources in the human brain*, Biomedical Engineering, IEEE Transactions on **BME-25** (1978), no. 5, 421–429.
- [19] Johannes Kepler; *Shape optimization with shape derivatives [J]*.
- [20] L. Ling, Y.C. Hon, M. Yamamoto; *Inverse source identification for poisson equation*, Inverse problems in science and engineering **13** (2005), no. 4, 433–447.
- [21] V. Morozov; *Methods of solving incorrectly posed problems*, Springer-Verlag, New York, 1984.
- [22] J. Nenonen, T. Katila, M. Leinio, J. Montonen, M. Makijarvi, P. Siltanen; *Magnetocardiographic functional localization using current multipole models*, Biomedical Engineering, IEEE Transactions on **38** (1991), no. 7, 648–657.
- [23] K. Ohnaka, K. Uosaki; *Boundary element approach for identification of point forces of distributed parameter systems*, International Journal of Control **49** (1989), no. 1, 119–127.
- [24] J. Sokolowski, J.P. Zolesio; *Introduction to shape optimization*, Introduction to Shape Optimization, Springer Series in Computational Mathematics, vol. 16, Springer Berlin Heidelberg, 1992, pp. 5–12 (English).
- [25] A. N Tikhonov; *On the stability of inverse problems*, Dokl.akad.nauk Sssr **39** (1943), no. 5, 176–179.
- [26] A. N. Tikhonov, A. V. Goncharsky, V. V. Stepanov, A. G. Yagola; *Numerical methods for the solution of ill-posed problems*, Kluwer Academic Publishers, 1995.

Ji-CHUAN LIU

SCHOOL OF MATHEMATICS, CHINA UNIVERSITY OF MINING AND TECHNOLOGY, XUZHOU, JIANGSU 221116, CHINA

E-mail address: liujichuan2003@126.com